IR Spectroscopic Characteristics of Cell Cycle and Cell Death Probed by Synchrotron Radiation Based Fourier Transform IR Spectromicroscopy

HOI-YING N. HOLMAN,[1] MICHAEL C. MARTIN,[2] ELEANOR A. BLAKELY,[3] KATHY BJORNSTAD,[3] WAYNE R. MCKINNEY[2]

[1] Center for Environmental Biotechnology, Lawrence Berkeley National Laboratory, One Cyclotron Road, Berkeley, California 94720

[2] Advanced Light Source Division, Lawrence Berkeley National Laboratory, One Cyclotron Road, Berkeley, California 94720

[3] Life Sciences Division, Lawrence Berkeley National Laboratory, One Cyclotron Road, Berkeley, California 94720

Received 18 February 2000; revised 19 April 2000; accepted 8 May 2000
Published online 19 September 2000

ABSTRACT: Synchrotron radiation based Fourier transform IR (SR-FTIR) spectromicroscopy allows the study of individual living cells with a high signal to noise ratio. Here we report the use of the SR-FTIR technique to investigate changes in IR spectral features from individual human lung fibroblast (IMR-90) cells *in vitro* at different points in their cell cycle. Clear changes are observed in the spectral regions corresponding to proteins, DNA, and RNA as a cell changes from the G_1-phase to the S-phase and finally into mitosis. These spectral changes include markers for the changing secondary structure of proteins in the cell, as well as variations in DNA/RNA content and packing as the cell cycle progresses. We also observe spectral features that indicate that occasional cells are undergoing various steps in the process of cell death. The dying or dead cell has a shift in the protein amide I and II bands corresponding to changing protein morphologies, and a significant increase in the intensity of an ester carbonyl C═O peak at 1743 cm^{-1} is observed. © 2000 John Wiley & Sons, Inc. Biopolymers (Biospectroscopy) 57: 329–335, 2000

Keywords: cell cycle; apoptosis; IR spectroscopy; synchrotron; Fourier transform IR; synchrotron radiation based Fourier transform IR spectromicroscopy

INTRODUCTION

Conventional Fourier transform IR (FTIR) spectroscopy and spectromicroscopy has been widely used as a diagnostic tool for characterizing the composition and structure of cellular components within intact tissues.[1–5] However, the spatial resolution of traditional FTIR spectromicroscopy is limited to ~75 μm with sufficient signal to noise at reasonably short data collection times.[6,7] Synchrotron radiation based FTIR (SR-FTIR) spectromicroscopy, on the contrary, provides several hundred times higher brightness at a nearly diffraction-limited spatial resolution of 10 μm or better (depending on wavelength) and is therefore a sensitive analytical technique capable of provid-

Correspondence to: H.-Y. N. Holman (hyholman@lbl.gov).
Contract grant sponsor: U.S. Department of Energy; contract grant number: DE-AC03-76SF00098.
Contract grant sponsor: Army Corps of Engineers, U.S. Department of Defense.
Contract grant sponsor: U.S. National Aeronautics Space Administration; contract grant number: T-965W.
Biopolymers (Biospectroscopy), Vol. 57, 329–335 (2000)

ing molecular information at a significantly finer spatial resolution on biological specimens. With this 10 μm or smaller spot size, SR-FTIR is ideally suited for the nondestructive, *in situ* study of processes that are taking place in individual cells. In a recent example, Jamin et al.[12] used SR-FTIR to map the distribution of functional groups of biomolecules such as proteins, lipids, and nucleic acids in individual live cells with a spatial resolution of a few microns. In this study we use SR-FTIR spectromicroscopy to investigate the spectral changes that occur in individual living human lung cells as a function of cell cycle and cell death.

MATERIALS AND METHODS

Cells and Cell Handling

The normal human fetal lung fibroblast IMR-90 P4 (P# indicates the passage number) cell line of female origin was obtained from the N.I.A. Cell Culture Repository, Coriell Institute for Medical Research.[13] Cells were cultured at 37°C in a 5% CO_2 environment in minimum essential medium with Earle's salts (Gibco/BRL) with 15% fetal calf serum (Hyclone), glutamine, Fungizone, PenStrep, and sodium bicarbonate (Gibco/BRL) in 75-cm^2 flasks. The IMR-90 P11 was plated at 8×10^5 cells in each 60-mm plastic petri dish 48 h prior to the experiment to insure the culture would double and grow to confluency as shown in the photograph in Figure 1(a). In this state the cells are ~82% synchronized into the G_1-phase of the cell cycle as detailed below.

Cells were rinsed 2 times in PBS, scraped, mixed, and pipetted onto dried, cleaned (acetone/deionized distilled water) gold-coated glass slide pieces (~0.5 $\times$ 0.5 cm) in 100-μL aliquots that were spread out with the pipette tip to insure single cells could be visualized. Slide pieces were placed on sterile gauze in the wells of a six-well plate prior to plating of the cells. The cells were allowed to settle and attach to the slide pieces for 30 min at 37°C in a 5% CO_2 incubator. After 30 min the cells were flooded with HEPES buffer-stabilized growth media to permit transport from the cell culture lab to the IR spectromicroscopy facility. The cell density was approximately 1.3×10^4 cells/cm^2 on the gold surface used for SR-FTIR analysis. A photomicrograph of cells ready for IR analysis is shown in Figure 1(b).

Fluorescence-activated cell sorting (FACS)[14–16] was used to measure the DNA content and therefore determine the distribution of cells in each phase of the cell cycle. The fractions of cells in the G_1-, S-, and G_2/M-phases were determined by staining cells fixed in 50% ethanol/PBS with propidium iodide and assaying 10^4 cells by flow cytometry using a Coulter Epics XL cytometer (Coulter Electronics, Miami, FL) with a 488-nm excitation source and a 575-nm emission filter; 10^4 cells of each sample were analyzed. Figure 2 shows the results of the FACS analysis, from which we determined that the IMR-90 cells grown to confluence consisted of 82.2% G_1-phase, 9.3% S-phase, and 8.5% G_2/M-phase. No cells of abnormal DNA content were observed.

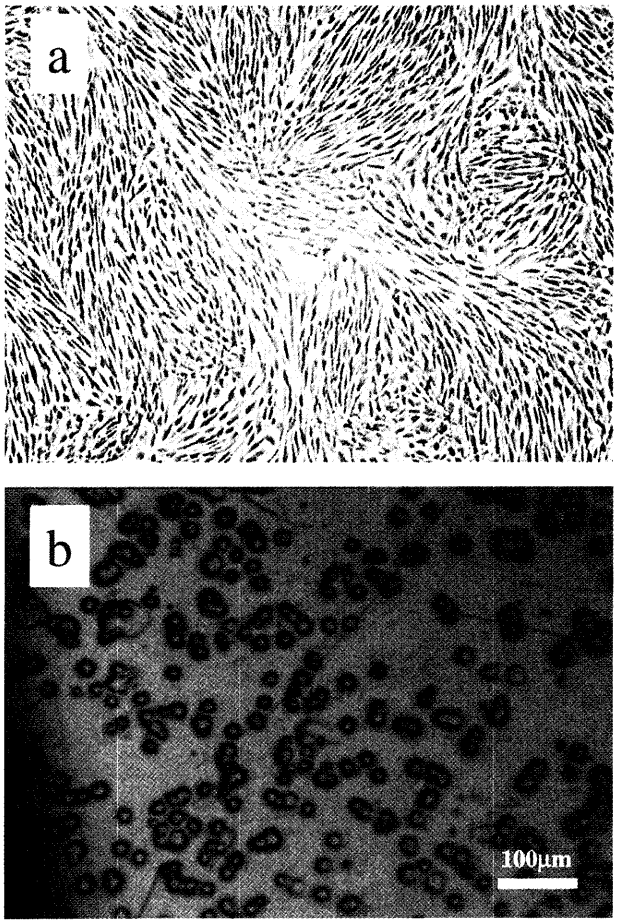

Figure 1. Digital phase photomicrographs of (a) IMR-90 cells grown to confluence on plastic with false coloring and (b) cells scraped off the plastic and allowed to attach to a gold-coated microscope slide for 0.5 h at 37°C. They are now ready for SR-FTIR analysis.

SR-FTIR Analysis

Spectromicroscopic measurements were made at beamline 1.4.3 at the Advanced Light Source, Lawrence Berkeley National Laboratory.[8,17–19]

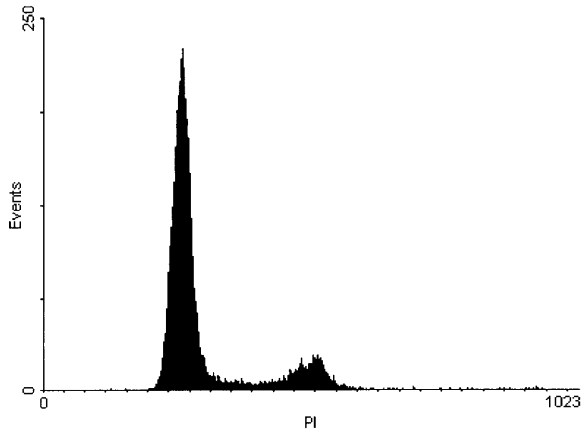

Figure 2. FACS analysis results for IMR-90 cells grown to confluence. The graph shows the distribution of cells as a function of DNA fluorescence, proportional to DNA content.

Synchrotron light from a bending magnet was collimated and then used as an external source for a Nicolet Magna 760 FTIR bench. The modulated beam was then directed into a Nic-Plan IR microscope where it was incident onto the sample stage, collected in reflectance or transmission mode, and finally directed onto a liquid nitrogen cooled mercury cadmium telluride detector.

The cells on the gold-coated glass were inserted into a small chilled chamber with a thin (~0.5 mm) IR-transparent ZnSe window to maintain a more constant humidity and prolong cell viability. Gold-coated slides were removed from the petri dishes. The sterile gauze was necessary to allow the slides to be easily removed from the bottom of the dish with minimal disturbance. Most of the liquid medium remaining on the surface of the slides was removed by carefully holding the slide at an angle against a piece of dry sterile gauze. The slide was then placed into a chamber situated on the motorized microscope stage. The chamber was chilled on ice before usage. A hole in the top piece of the chamber had a provision for a ZnSe IR-transparent window.

Data for this study was acquired in the double-pass transmission mode. (The IR beam passes through a cell and is again reflected back from the gold surface through the cell.) The sample stage was moved to align the center of the cell of interest with the focused SR-IR spot to within a few microns. Spectra were typically obtained from an individual cell using 4 cm^{-1} resolution and 64 co-added interferograms. On the order of 100 individual cells were measured, which were spread through the various morphologies. No apertures were used in the beam from the source to the sample; therefore, the approximately diffraction-limited spot size in the mid-IR region of interest was always 10 μm or less.

RESULTS

Cell Cycle Spectra

The cell division cycle consists of four major stages denoted G_1-, S-, G_2-, and M-phases.[20] During the S-phase the DNA is replicated to form two complete copies of the cell's genes in preparation for division during the M-phase.

Visual inspection of the cell size and morphology in the IR microscope at 320× magnification showed that the majority of the IMR-90 cells were spheres ~10 μm in diameter. We identified these cells as being in the G_1-phase by comparison with the FACS data above. Occasionally slightly elliptical cells, which were clearly distinguishable from grossly deteriorating cells, were found to be considerably larger (~30 μm). Other cells were found to be in between the two extremes in size, typically ~15 μm. We tentatively identified the largest cells as being in the G_2-phase or undergoing M (G_2/M-phase) and the in between sizes as being in the S-phase.

We found that cells tentatively identified as being in the G_1-, S-, and G_2/M-phase of the cycle showed clearly different spectra. Figure 3 shows the 1800–900 cm^{-1} region for typical individual cells in each of these three phases. These spectra are not normalized. Cell to cell spectral variations within each cell cycle phase were significantly smaller than the phase to phase changes reported here. During the S-phase the DNA was undergoing replication and we observed that the absorptions in the DNA/RNA spectral region increased relative to the G_1-phase spectra by approximately a factor of 2. We also noted that the centroid positions of the amide I and II peaks shifted down in energy as listed in Table I.

When a G_2/M-phase cell was measured we observed a large increase in the overall absorbance (uppermost spectrum in Fig. 3). This may have been a result of more material in the cell or because the thickness may have been different in the M-phase. In the second case there could have been a greater path length for the IR beam to traverse. Other more complicated mechanisms may have also been active, including the conden-

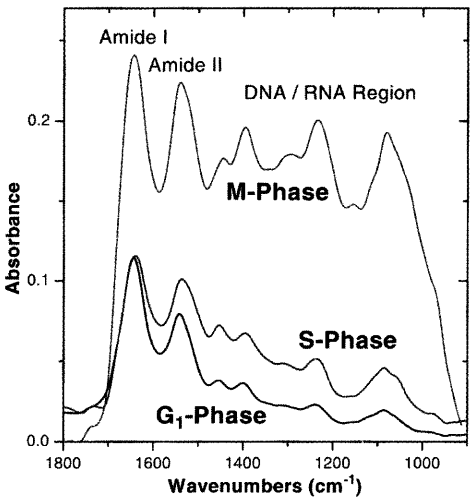

Figure 3. IR spectra of individual cells in different stages of the cell cycle. The spectra were not normalized, but a linear baseline was subtracted over the range of 2000–650 cm^{-1}.

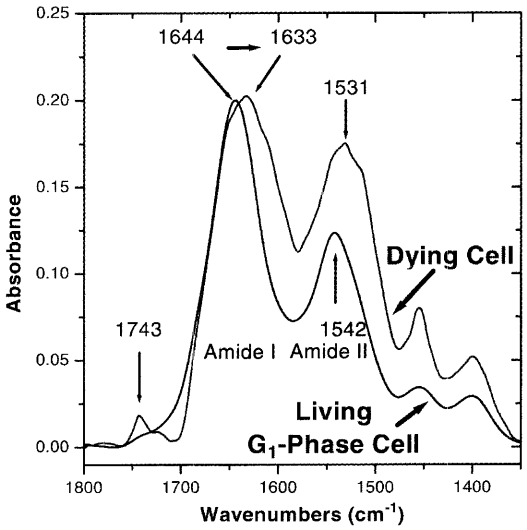

Figure 4. An IR spectra comparison of individual living and dying cells. The spectra were normalized to the amide I peak, and a linear baseline was subtracted in the range of 1800–1350 cm^{-1}.

sation of chromatin during these phases of the cell cycle. Absorptions in the DNA/RNA region were significantly increased relative to the protein peaks. It was also noteworthy that the peak around 1395 cm^{-1} was noticeably larger in the G_2/M-phase than in the other phases.

Dying Cell Spectra

Occasionally some cells exhibited different spectral characteristics near the protein amide I and II peaks, even though the cell's morphology did not appear different visually. Comparing these spectra to recently presented research on lysed necrotic cells,[12,21] we see that the spectral changes observed indicate that the cells were dying or dead. The spectrum of one such cell is shown in Figure 4 along with the spectrum of a normal living G_1-phase cell. The "dying" cell shows two characteristic spectral signatures indicative of death.[12,21] First, the centroids of the protein amide I and II peaks shift from 1644 to 1633 and 1542 to 1531 cm^{-1}, respectively, indicating a change in the overall protein conformational states within the cell. Second, we observe the appearance of a peak at around 1743 cm^{-1}. These observations can now be used as signatures of cell death in future studies.

We also measured a number of cells that had no visually intact cell membranes. Spectra from these cells were similar to those reported by Jamin et al.[12] and Miller[21] in that a peak at ~1728 cm^{-1} became prominent with a shoulder at ~1743 cm^{-1}. The amide peaks were also observed to shift down to lower energies with the exact amount of the shifts varying from cell to cell.

Table I. Peak Positions for G_1-, S-, and M-Phase Cells (cm^{-1})

Peak	G_1-Phase	S-Phase	M-Phase
Amide I	1644	1640	1644
Amide II	1542	1536.5	1540

DISCUSSION

Cell Cycle Spectra

We used SR-FTIR spectromicroscopy to obtain IR spectra from individual cells, which clearly show characteristic spectral differences for different phases of the cell cycle. A previous study looked at the average IR absorption response of human myeloid leukemia cells, which were separated into G_1, S, and G_2 cell cycle stages by centrifugal elutriation, either macroscopically by measuring ~10^4 cells or microscopically by averaging the response of 10–50 individual cells measured using a conventional IR source and a 15-μm aper-

ture in an IR microscope.[1,22] They were unable to separate and measure cells in the M-phase because of the short time their cells spent in that phase (<4% of the cell division cycle is in the M-phase).

Our G_1- and S-phase results in Figure 3 (each from a single cell) confirm the bulk ($\sim 10^4$ cells) and the combined single cell (10–50 cells) measurements of Diem et al.[1] and Boydston-White et al.[22] We observed that the intensity of the DNA/RNA spectral region peaks relative to the protein amide peak intensities was markedly increased in the S-phase compared to the G_1-phase. Because the DNA is replicated throughout the S-phase, it is reasonable to expect a greater DNA signal in the IR spectra. Alternatively, Diem et al.[1] and Boydston-White et al.[22] hypothesized that in the G phases the DNA is packed so tightly into nucleosomes that the IR absoptions are optically thick and will therefore be unobservable in the IR spectra. However, during the S-phase, portions of the DNA are packed less densely and therefore will contribute to the IR spectrum.[1,22] In our S-phase spectrum the PO_2^- peak at ~ 1085 cm^{-1} showed a small "nose" consistent with the spectrum of RNA.[22,23] Further studies are necessary to fully assess whether DNA/RNA packing and/or content is responsible for the increased IR absorption observed.

We also observed that the centroid positions of the protein amide I and II peaks shifted to lower energy in the S-phase compared to the G_1-phase as shown in Table I. Using a simple amide peak shape interpretation, these shifts were consistent with more cellular proteins having a β-sheet secondary structure in the S-phase compared to a higher α-helix protein content in the G_1-phase.[2,3,24–26]

The uppermost trace in Figure 3 is significantly different from the G_1- or S-phase spectra. Diem et al.[1] and Boydston-White et al.[22] showed that their G_2-phase cells had spectra very similar to those in the G_1-phase. Therefore, we concluded that our measured cell was in the M-phase and not in the G_2-phase. To our knowledge, the top curve in Figure 3 presents the first measured M-phase IR spectrum from a mitotic cell. The overall absorption intensity in the DNA/RNA spectral region increased significantly relative to the protein amide vibration peaks. Because the DNA is more tightly packed into chromosomes during the M-phase,[20] the optical density arguments of Diem et al.[1] and Boydston-White et al.[22] would point toward this enhancement being due to RNA in the cell. Because the nucleolus disappears during M-phase with the presumed dispersal of the associated RNA and ribosomes, a straightforward interpretation would be that the dispersed RNA is now optically thinner and contributes more to the IR spectrum. However, the ratio of the ~ 1085 cm^{-1} PO_2^- to ~ 1230 cm^{-1} phosphodiester and amide III peaks is closer to that of DNA. The full understanding of this complex behavior will require further study and interpretation.

The centroid positions of the amide I and II peaks in the M-phase returned to wavelengths that primarily correlated to the secondary structures of the α helices, similar to the G_1-phase results, as listed in Table I. The amide I peak completely returned to the G_1-phase position while the amide II peak stopped 2 wavenumbers short of a full return.

The M-phase spectrum also showed that the absorption mode at ~ 1395 cm^{-1} was much enhanced compared to the G_1- and S-phase spectra. Because this one peak grew much more than the overall protein, DNA/RNA, or lipid (not shown) spectral regions, we can conclude that this growth was not simply related to the amount or density of these major cellular components. Absorptions affected by helical conformations of DNA, as well as protein side chain vibrations, are components to this spectral region.[27] Thus, future detailed experiments are required to assign this intensity growth to a specific phenomenon.

Dying Cell Spectra

The spectrum of a dying cell (Fig. 4) shows significant shifts in the amide I and II peaks compared to the spectrum of a living cell. As a first (overly simplistic) analysis we fitted the amide I peak shape in the living and dying cell spectra to a series of empirically determined peak positions for the various secondary structures of proteins.[2,3,24–26] When we compared the amplitudes of the three nominal "β-sheet" subcomponents at 1605, 1623, and 1667 cm^{-1} to the central α-helix component at 1640 cm^{-1}, we found that the amount of β-sheet secondary structures increased by $\sim 20\%$ in the dying cell compared to the living cell. The amount of "random coils" was only increased by $\sim 2\%$ in the dying cell. These structural changes in the cellular proteins could be due to a different distribution of proteins during apoptosis or to denaturation of the existing proteins. This analysis is simplistic and ignores other spec-

tral features under the amide I envelope such as ring breathing and C=O stretching vibrations of DNA and RNA. Furthermore, Torii and Tasumi[28] demonstrated that the interpretation of amide I envelopes requires more than simple deconvolution with spectral features from a "basis set" of model proteins. Their analysis of the IR spectrum of myoglobin, which has no β-sheet secondary structures, shows that the amide I peak can have weaker absorption in the nominal β-sheet wavelength region of a simple model.

The new peak at ~1743 cm^{-1} in the dying cell is usually associated with the non-hydrogen-bonded ester carbonyl C=O stretching mode within phospholipids.[5,29,30] We did not see a large increase in other lipid absorption bands in the dying cell, so this peak was not simply an increase in the number of lipid molecules or their density. A shoulder at ~1725 cm^{-1} was also observed, which is associated with hydrogen-bonded C=O groups.[29] An increase in a peak at this position was seen by Jamin et al.,[12] although in that study the authors investigated a cell that had experienced necrosis and was visually changed morphologically because of a loss of cell membrane integrity.[31] When we investigated IMR-90 cells that had lost membrane integrity, we observed results similar to those of Jamin et al.[12] The fact that the ~1743 cm^{-1} peak in Figure 4 is significantly more intense than the ~1725 cm^{-1} peak implies that the C=O ester carbonyl groups of lipids in the cell are becoming predominantly non-hydrogen bonded, which would be in agreement with oxidative damage having occurred. Apoptosis is associated with, among other factors, increased oxidative damage.[32,33] Therefore, the cell we measured may have been in the early stages of apoptosis and not a lysosomal type of death whereas cells visually observed to have lost membrane integrity were most likely lysosomal and had different IR spectral characteristics.

It is also interesting to note that the peak at ~1455 cm^{-1} became much sharper than was observed in any of the living cell cycle phase measurements. A vibration due to protein side chains was approximately at this position, as well as some DNA/RNA and lipid vibrational modes. However, Venyaminov et al.[34] state that only the pH or mutations can change vibrations from protein side chains. At present it is not clear which cellular component causes this sharpened feature.

CONCLUSIONS

We presented IR spectra obtained from individual living human lung fibroblast cells as a function of cell cycle phase, as well as spectra for a cell that was dying or dead. We found very significant differences in the spectra that need to be understood and taken into account when making comparisons of IR spectra from normal and moribund cells. The power of using a synchrotron based IR source was demonstrated where data from one individual cell without any fixing, staining, or labeling provided excellent signal to noise. More importantly, we showed that these single cell SR-FTIR spectra were of sufficient quality and reproducibility to allow detailed interpretation in terms of specific molecular events.

Future research will build upon previous IR studies and complement other microscopy and biochemistry techniques to investigate changes in many different types of cells, as well as cellular biochemical processes resulting from a variety of agents. Although the IR spectra of whole cells are quite complex, the use of cell lines that are defective in a single process or pathway may allow the identification of key spectral features associated with important biochemical and physiological mechanisms. With sufficient development IR spectromicroscopy may become a rapid and inexpensive diagnostic tool for medical screening applications. In addition, the single cell nature of the SR-FTIR technique will allow reliable detection and identification of a small number of cells within a sample that are different from the others, potentially opening new areas of environmental health and biomedical research.

REFERENCES

1. Diem, M.; Boydston-White, S.; Chiriboga, L. Appl Spectrosc 1999, 53, 148A–161A.
2. Stuart, B.; Ando, D. J. Biological Applications of Infrared Spectroscopy. Wiley: Chichester, UK, 1997 [published on behalf of ACOL, University of Greenwich].
3. Mantsch, H. H.; Chapman, D. Infrared Spectroscopy of Biomolecules; Wiley–Liss: New York, 1996.
4. Griffiths, P. R.; De Haseth, J. A. Fourier Transform Infrared Spectrometry. Chemical Analysis; Wiley: New York, 1986; Vol. 83.
5. Parker, F. S. Applications of Infrared Spectroscopy in Biochemistry, Biology, and Medicine; Plenum: New York, 1971.
6. Choo, L.-P. I.; Wetzel, D. L.; Halliday, W. C.; Jack-

son, M.; Levine, S. M.; Mantsch, H. H. Biophys J 1996, 71, 1672–1679.
7. Carr, G. L.; Reffner, J. A.; Williams, G. P. Rev Sci Instrum 1995, 66, 1490–1492.
8. Martin, M. C.; McKinney, W. R. In Application of Synchrotron Radiation Techniques to Materials Science IV; Mini, S. M., Stock, S. R., Perry, D. L., Terminello, L. J., Eds.; Materials Research Society: San Francisco, 1998; Vol. 524, pp 11–15.
9. Miller, L. M.; Carr, G. L.; Williams, G. P.; Chance, M. R. Biophys J 1997, 72, A214.
10. Lappi, S.; Miller, L.; Chance, M.; Franzen, S. Biophys J 1999, 76, A354.
11. Holman, H.-Y. N.; Goth-Goldstein, R.; Martin, M. C.; Russell, M. L.; McKinney, W. R. Environ Sci Technol 2000, 34, 2513–2517.
12. Jamin, N.; Dumas, P.; Moncuit, J.; Fridman, W.-H.; Teillaud, J.-L.; Carr, G. L.; Williams, G. P. Proc Natl Acad Sci USA 1998, 95, 4837–4840.
13. Nichols, W. W.; Murphy, D. G.; Cristofalo, V. J.; Tiji, L. H.; Greene, A. E.; Dwight, S. A. Science 1977, 196, 60–63.
14. Crissman, H. A.; Darzynkiewicz, Z.; Tobey, R. A.; Steinkamp, J. A. Science 1985, 228, 1321–1324.
15. Czerniak, B.; Darzynkiewicz, Z.; Herz, F.; Wersto, R. P.; Koss, L. G. Mater Med Polona 1989, 21, 3–9.
16. Chang, Y.-Y. Radiat Res 1996, 146, 494–500.
17. Further information on the Advance Light Source IR beamlines is at http://infrared.als.lbl.gov/.
18. McKinney, W. R.; Martin, M. C.; Byrd, J. M.; Miller, R.; Chin, M.; Portman, G.; Moler, E. J.; Lauritzen, T.; McKean, J. P.; West, M.; Kellogg, N.; Zhuang, V.; Ross, P. N.; Ager, J. W.; Shan, W.; Haller, E. E. In Accelerator-Based Sources of Infrared and Spectroscopic Applications; Carr, G. L., Dumas, P., Eds.; SPIE Proceedings: Denver, CO, 1999; Vol. 3775, pp 37–45.
19. McKinney, W. R.; Hirschmugl, C. J.; Padmore, H. A.; Lauritzen, T.; Andresen, N.; Andronaco, G.; Patton, R.; Fong, M. In Accelerator-Based Infrared Sources and Applications; Williams, G. P., Dumas, P., Eds.; SPIE Proceedings: San Diego, CA, 1997; Vol. 3153, pp 57–65.
20. Becker, W. M.; Reece, J. B.; Poenie, M. F. The World of the Cell; Benjamin Cummings: Menlo Park, CA, 1996; 3rd ed.
21. Miller, L. personal communication, 1999.
22. Boydston-White, S.; Gopen, T.; Houser, S.; Bargonetti, J.; Diem, M. Biospectroscopy 1999, 5, 219–227.
23. Tsuboi, M.; Takahashi, S.; Harada, I. In Physico-Chemical Properties of Nucleic Acids; Duchesne, J., Ed.; Academic: London, 1973; p 91.
24. Byler, D. M.; Susi, H. Biopolymers 1986, 25, 469–488.
25. Haris, P. I.; Chapman, D. Trends Biochem Sci 1992, 7, 328–333.
26. Surewicz, W. K.; Mantsch, H. H. Biochim Biophys Acta 1988, 952, 115–130.
27. Liquier, J.; Taillandier, E. In Infrared Spectroscopy of Biomolecules; Mantsch, H. H., Chapman, D., Eds.; Wiley–Liss: New York, 1996; pp 131–158.
28. Torii, H.; Tasumi, M. In Infrared Spectroscopy of Biomolecules; Mantsch, H. H., Chapman, D., Eds.; Wiley–Liss: New York, 1996; pp 1–18.
29. Fabian, H.; Chapman, D.; Mantsch, H. H. In Infrared Spectroscopy of Biomolecules; Mantsch, H. H., Chapman, D., Eds.; Wiley–Liss: New York, 1996; pp 341–352.
30. Jackson, M.; Mantsch, H. H. In Infrared Spectroscopy of Biomolecules; Mantsch, H. H., Chapman, D., Eds.; Wiley–Liss: New York, 1996; pp 311–340.
31. Zakeri, Z. In When Cells Die: A Comprehensive Evaluation of Apoptosis and Programmed Cell Death; Lockshin, R. A., Zakeri, Z., Tilly, J. L., Eds.; Wiley–Liss: New York, 1998; pp 97–129.
32. Mittler, R. In When Cells Die: A Comprehensive Evaluation of Apoptosis and Programmed Cell Death; Lockshin, R. A., Zakeri, Z., Tilly, J. L., Eds.; Wiley–Liss: New York, 1998; pp 147–174.
33. Birge, R.; Fajardo, E.; Hempstead, B. In When Cells Die: A Comprehensive Evaluation of Apoptosis and Programmed Cell Death; Lockshin, R. A., Zakeri, Z., Tilly, J. L., Eds.; Wiley–Liss: New York, 1998; pp 347–384.
34. Venyaminov, S. Y.; Braddock, W. D.; Prendergast, F. G. Biophys J 1996, 70, A65.

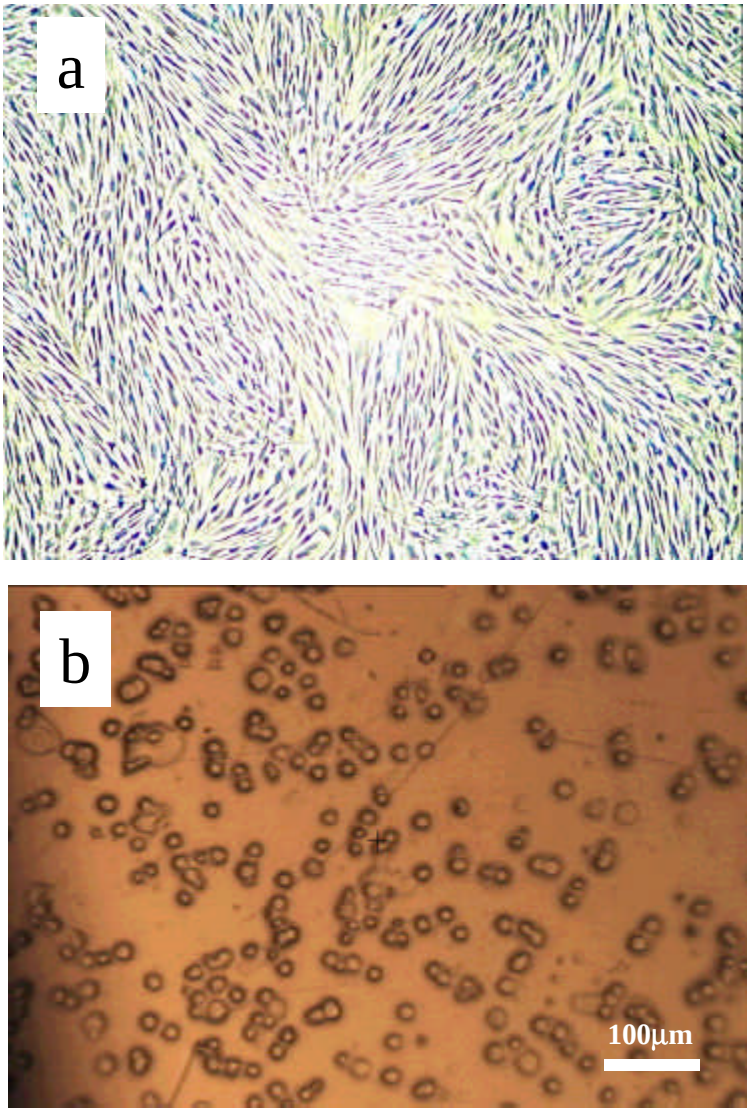

Figure 1. (a) Digital phase photomicrograph of IMR-90 cells grown to confluence on plastic with false coloring. (b) Digital photomicrograph of cells scraped off of the plastic and allowed to attach to a gold-coated microscope slide for half an hour at 37°C. They are now ready for SR-FTIR analysis.